Published in final edited form as:
Anal Chem. 2012 April 17; 84(8): 3607–3613. doi:10.1021/ac203375d.

Imaging the Material Properties of Bone Specimens using Reflection-Based Infrared Microspectroscopy

Alvin S. Acerbo, **G. Lawrence Carr**, **Stefan Judex**, and **Lisa M. Miller***
Photon Sciences Directorate, Brookhaven National Laboratory, Upton, NY 11973 United States and Department of Biomedical Engineering, Stony Brook University, Stony Brook, NY 11794 United States

Abstract

Fourier Transform InfraRed Microspectroscopy (FTIRM) is a widely used method for mapping the material properties of bone and other mineralized tissues, including mineralization, crystallinity, carbonate substitution, and collagen cross-linking. This technique is traditionally performed in a transmission-based geometry, which requires the preparation of plastic-embedded thin sections, limiting its functionality. Here, we theoretically and empirically demonstrate the development of reflection-based FTIRM as an alternative to the widely adopted transmission-based FTIRM, which reduces specimen preparation time and broadens the range of specimens that can be imaged. In this study, mature mouse femurs were plastic-embedded and longitudinal sections were cut at a thickness of 4 μm for transmission-based FTIRM measurements. The remaining bone blocks were polished for specular reflectance-based FTIRM measurements on regions immediately adjacent to the transmission sections. Kramers-Kronig analysis of the reflectance data yielded the dielectric response from which the absorption coefficients were directly determined. The reflectance-derived absorbance was validated empirically using the transmission spectra from the thin sections. The spectral assignments for mineralization, carbonate substitution, and collagen cross-linking were indistinguishable in transmission and reflection geometries, while the stoichiometric/non-stoichiometric apatite crystallinity parameter shifted from 1032 / 1021 cm^{-1} in transmission-based to 1035 / 1025 cm^{-1} in reflection-based data. This theoretical demonstration and empirical validation of reflection-based FTIRM eliminates the need for thin sections of bone and more readily facilitates direct correlations with other methods such nanoindentation and quantitative backscatter electron imaging (qBSE) from the same specimen. It provides a unique framework for correlating bone's material and mechanical properties.

Keywords

Fourier transform infrared microspectroscopy; imaging; bone composition; mineralized tissue; Kramers-Kronig transformation; specular reflection

INTRODUCTION

The tissue material properties of bone are important contributors to bone quality and fracture risk.[1-3] In particular, mineralization, crystallinity, and collagen cross-linking may play a role

*To whom correspondence should be addressed, lmiller@bnl.gov.
Authors' roles: Study design: LM, AA, SJ. Data collection: AA. Data analysis: AA and GC. Data interpretation: AA, GC, SJ, and LM. Drafting manuscript: AA and LM. Revising manuscript content: AA, GC, SJ, and LM. Approving final version of manuscript: AA, GC, SJ, and LM. LM takes responsibility for the integrity of the data analysis.

SUPPORTING INFORMATION AVAILABLE
Additional information as noted in the text. This material is available free of charge via the Internet at http://pubs.acs.org.

in defining bone's mechanical properties. For example, positive correlations have been observed between mineralization and Young's modulus in aging mice,[2] newborn rabbits,[4] osteons of baboons,[5, 6] the secondary mineralization of ewes,[7] estrogen and bisphosphonate-treated rats,[8] and vitamin D-deficient rats.[3] In humans, fracture risk has recently been associated with mineralization in cortical but not trabecular bone of the iliac crest,[9] the latter of which was altered by bisphosphonate treatment.[10] While it is clear that bone's chemical, mechanical, and morphological parameters all contribute to the mechanical behavior of bone, specific relationships are often difficult to identify, in particular when the analytical methods have different constraints related to tissue preparation, and assess bone's complex material properties at different hierarchical levels and in different volumes of the tissue.

Fourier transform infrared microspectroscopy (FTIRM) and imaging (FTIRI) have become the most widely used techniques for determining the spatially-resolved chemical makeup of bone. To date, FTIRM has required thin sections of bone (typically <5 μm) in order to provide sufficient transmission of infrared (IR) light through the tissue. Specimens that are too thick will cause insufficient illumination of the detector and prevent an accurate measurement, making quantitation impossible. Moreover, thin sections require bones to be embedded in an infiltrating plastic resin that can alter the chemical composition and cause spectral overlap with absorption features of bone.[11, 12] Spectral subtraction can be performed using a pure spectrum of the embedding material, but this can introduce error into the data since the embedding material may not be distributed homogeneously throughout the specimen. But perhaps the most important limitation of transmission-based FTIRM is the inability to perform correlative studies on the same specimen with other biomechanical and morphological methods, e.g. nanoindentation, qBSE, and 2-D surface slices from μCT reconstructions, due to the differences in specimen preparation.

In this work, we demonstrate the theoretical development and empirical validation of reflection-based FTIRM. In a reflection geometry, IR spectra are generated based on the specular reflection of IR light from a polished surface, thereby removing the requirement for thin specimens. The resultant spectra can be transformed into absorbance spectra through a Kramers-Kronig relationship. In addition to the theoretical treatment of this method, we have performed an empirical validation with transmission-based FTIRM on the corresponding thin sections of bone. With this reflection method, FTIRM can now be expanded to the analysis of thick specimens and blocks of bone, enabling direct, pixel-to-pixel correlation on the same specimen with other biomechanical and morphological imaging data.

METHODS

Specimen Preparation

Three poly-methyl methacrylate (PMMA)-embedded mature mouse femurs were provided by Dr. David Burr (Indiana University School of Medicine). From each block, three longitudinal serial sections were cut from the mediolateral plane at a thickness of 4 μm ± 0.35 μm. The second section for each femur was mounted in a slotted aluminum frame for transmission-based FTIRM. The corresponding bone blocks were first imaged unpolished with reflection-based FTIRM and then polished (Buehler, Lake Bluff, IL) with 1,200 grit carbide paper and a cloth impregnated with diamond suspensions (particle size 3, 1, 0.25, 0.05 μm) for 3 min at each step, removing a total of 54 ± 12 μm of material from the specimen surface. The polished bone blocks were then imaged. Thus, the thin section for transmission was located ~4 μm from the unpolished surface and ~60 μm from the polished surface.

FTIRM Data Collection

FTIRM data were collected using a Nicolet Continuμm IR microscope (Thermo Electron Corp) at beamline U2B of the National Synchrotron Light Source at Brookhaven National Laboratory. Spectra were collected in the mid-IR region from 4000 - 650 cm^{-1} using a MCT-A* (Mercury Cadmium Telluride) detector, at a spectral resolution of 8 cm^{-1} and 128 scans/pixel. FTIRM mapping was performed with the synchrotron source, using an aperture size of 15 × 15 μm and a step size of 15 μm. Specimens were oriented such that the incident IR beam was 90% s-polarized. For each femur, a 300 μm longitudinal section of the cortical shell in the mid-diaphysis was imaged with a conventional light microscope, where matching locations were identified for both the bone blocks and the corresponding thin sections. For the thin sections, data were collected in a transmission geometry, where the background spectrum was collected through an empty specimen holder. For the bone blocks, data were collected in a specular reflection geometry from the top surface of the specimen. A polished CsI disk was used as the reflectance background to produce a detector signal comparable to that from the specimen itself, thereby reducing susceptibility to detector non-linearity. We note that CsI has no spectral features in the spectral range of interest (4000 - 650 cm^{-1}) and that spectra can be readily corrected to a 100% reference value using its known optical properties. For each specimen, 250 - 300 spectra were collected and normalized to the synchrotron beam current.

In order to accurately employ the Kramers-Kronig transformation to the reflection-based data, a template bone IR spectrum was also collected over the far-IR to mid-IR region (4000 - 70 cm^{-1}) from a different polished mouse bone block. The 4000 - 650 cm^{-1} spectral range was collected with the Nicolet Continuμm IR microscope as described above. A Spectra Tech IRμs microscope was used at beamline U12IR at the National Synchrotron Light Source. A bolometer and photoconductive Ge:Cu detector were used to obtain data over the 400 - 70 cm^{-1} and 1000 - 200 cm^{-1} spectral ranges, respectively. Reflection-based data were collected from the top surface of the bone block with the synchrotron source and an aperture size of 120 × 120 μm (8 cm^{-1} resolution, 1024 scans/pixel). Overlapping spectral regions were observed to be identical and were manually removed. The three spectra were then appended to produce a continuous template bone IR spectrum from 4000 - 70 cm^{-1}.

Chemical Parameters

Bone chemical composition parameters were determined from the transmission and reflection-derived absorbance spectra using Bruker OPUS 6.5 software. Specifically, we determined the degree of mineralization (phosphate / protein ratio),[13] carbonate substitution into the mineral lattice (carbonate / phosphate ratio),[14] crystallinity (ratio of stoichiometric / non-stoichiometric phosphate),[15] and collagen cross-linking[16] as outlined in Table 1.

Statistical Analyses

Means, standard deviations, and the ratio of the standard deviation to the mean (i.e. coefficients of variation) for each integration map were calculated. Edge pixels were identified by overlaying the IR map with the visible light micrograph and were discarded from the data set. Values for percent difference between the thin sections and polished blocks were calculated by dividing the difference between the means by the average of the means.

RESULTS

Transmission-based FTIRM

IR absorbance spectra of bone were collected in a transmission geometry through 4 μm bone thin sections (Figure 1). In most regions, the specimens were cut sufficiently thin to permit

at least 10% transmission of the IR light as to ensure a linear response from the detector. The resultant spectra from these regions showed well-defined absorption peaks. Local regions where the sections were too thick (typically >5 μm) had zero or near-zero transmission, resulting in spectra with truncated or ill-defined absorbance values in spectral regions with high absorbance, most notably the $\nu_1, \nu_3 PO_4^{3-}$ region from 1200 - 900 cm^{-1}. Furthermore, several spectra appeared to contain absorption peaks unique to the PMMA embedding material. PMMA has major absorption features that overlap with the protein, carbonate, and mineral phosphate peaks found in bone, and is most easily recognized by a sharp and intense carbonyl ester absorption peak centered at 1745 cm^{-1} (Figure 1).

Reflection-based FTIRM

As an alternative to transmission-based FTIRM, the chemical composition of bone was assessed using a specular reflection geometry, where reflected IR light is collected from the bone surface at a near-normal angle. In a specular reflectance spectrum, absorption features have a derivative-like appearance due to a combination of the specimen's dispersive refractive index and extinction coefficient[17] (Figure 2A). Although all of the absorption features exist in this spectrum, the conventional analysis method for transmission spectral data is not appropriate. To analyze the reflectance spectral data, we used a standard method based on a Kramers-Kronig relationship to directly extract the specimen's complex refractive index. Other quantities, such as the absorbance, were then calculated and used in the same manner as spectral data from the transmission geometry.

The Kramers-Kronig relationships connect the real and imaginary parts of any physical response function by an integral transform. When a light wave is incident on a surface, a portion is reflected and also shifted in phase. A measurement of the reflectance can evaluate the reflected wave amplitude, but not the phase shift. Applying the Kramers-Kronig transformation to the measured reflected wave amplitude yields the phase shift. Knowing both the reflected wave amplitude and phase shift is sufficient to uniquely determine the material's refractive index, from which other quantities, such as the absorption coefficient, can be directly derived. The resulting frequency-dependent absorption coefficient can then be analyzed using standard transmission spectroscopy methods (see Supporting Information).

One challenge of the Kramers-Kronig transform is that it involves integrations over all spectral frequencies from zero to infinity. Fortunately, the contributions from distant spectral regions become insignificant and simple extrapolations for the reflectance can be used to good accuracy. However, it is important to capture any nearby spectral features; therefore, measurements must cover a sufficiently broad spectral range to ensure this is achieved. For bone, most of the dominant spectral features occur from 2000 - 500 cm^{-1}. Thus, in order for the Kramers-Kronig transformation to be applied accurately, each bone spectrum must be extended beyond this spectral range.

Conventional FTIR microscopes use MCT detectors that have a good spectral response from approximately 4000 to 650 cm^{-1}. When the Kramers-Kronig transformation was applied to a bone spectrum having a low-frequency cutoff of 650 cm^{-1}, the resulting $\nu_1,\nu_3\ PO_4^{3-}$ absorption peak from 1200 - 900 cm^{-1} had an incorrect (i.e. skewed) baseline (Figure 2B). While the intensity and frequency of the $\nu_1,\nu_3 PO_4^{3-}$ peak are correct, the skewed baseline can cause significant error during peak integration. Extending the measured spectral range down to 450 cm^{-1} improved the baseline. However, due to the $\nu_4\ PO_4^{3-}$ peak from 650 - 500 cm^{-1}, the bone spectrum should be extended even further in order to completely account for these absorbance features prior to applying the Kramers-Kronig transformation. Figure 2B also shows a bone spectrum that was collected to 70 cm^{-1}. This spectrum clearly shows that the baselines for both the ν_1,ν_3 and the $\nu_4\ PO_4^{3-}$ peaks are no longer skewed.

Thus, in order to generate accurate reflection FTIRM data, the bone spectral range should ideally be at least 4000 - 70 cm^{-1}.

In practice, conventional FTIR microscopes are not equipped with the appropriate detectors for collecting this wide spectral range. However, an *a priori* knowledge of the absorption features of bone permits spectral extrapolation without the need to collect data to 70 cm^{-1}. Thus, we collected a reflection spectrum across the mid- and far-IR spectral range (4000 - 70 cm^{-1}) from a different polished bone specimen. This template spectrum was used to extend the spectral range of spectra collected with the conventional MCT detector from 850 to 70 cm^{-1}. Specifically, a Matlab routine was developed to scale the 4000 - 2500 cm^{-1} baseline region of the template spectrum to match that of the specimen spectra and the ν_1,ν_3 PO_4^{3-} peak intensity at 1035 cm^{-1} of the template was scaled to match that of the specimen spectra. Then, the 850 - 70 cm^{-1} portion of the template spectrum was appended to the specimen spectra, and the 900 - 850 cm^{-1} region of the specimen spectra were replaced with an averaged 900 - 850 cm^{-1} region from the template spectrum and the specimen spectra. The OPUS 6.5 (Bruker Optics, Billerica, MA) Kramers-Kronig transform algorithm was used to calculate the extinction coefficient of extended specimen spectra spanning 4000 - 70 cm^{-1}. From there we determined frequency-dependent absorption coefficient spectra assuming a 4 μm thick specimen (see Supporting Information).

Surface polishing to maximize specular reflectance

Polishing of the specimen surface with a particle grit size of 50 nm yielded an increase in bone reflectance of up to 10% (Figure 3A). Most notably, the ν_1,ν_3 PO_4^{3-} region saw an increase in reflection from 5% to 15% after polishing. This gain in reflectance translated into a higher amplitude absorption coefficient spectrum and improved signal-to-noise of the spectral absorption peaks (Figure 3B). It is important to note that a poorly polished surface may lead to a mainly diffuse reflecting surface and an overall reduction in the reflected signal, resulting in poor signal-to-noise. However, the relative absorption strengths for the various spectral features are not affected, such that accurate chemical information can still be obtained. Although polishing has the potential to alter the chemical composition of the bone surface, these changes are likely small and limited to an undetectable fraction of the sampled depth by reflection-based FTIRM.

The effect of angle of incidence & light polarization

The intensity of light reflected back from the bone surface is referred to as the reflection coefficient, which is a function of the refractive index of bone, the angle of incidence, and the polarization of the light. Normal incidence is assumed for the conventional Kramers-Kronig transform algorithm, which is a potential issue for reflectance measurements using a high numerical aperture optic where angles of incidence can approach 40°. To test this issue, the reflection coefficient of fully mineralized bone was estimated as a function of incident angle and polarization using the refractive index of hydroxyapatite (n = 1.530). For Schwarzschild objectives typically used in IR microscopes (numerical aperture: ~0.6), the incidence half angle range was determined to be 15 - 40° with a median of 37° (Figure 4A). Using the Fresnel equations for both *s*- and *p*-polarized light, it was determined that the reflection coefficient for hydroxyapatite was sufficiently constant out to 40° that it did not measurably affect the analysis. The other specimen constituents had a smaller refractive index for which the angle dependence was even weaker (Figure 4B). Thus, for the standard FTIRM configuration, the angle of incidence was close enough to the normal such that the reflection coefficient remained approximately constant for all types of polarization.

Validation of reflection-based FTIRM with transmission-based FTIRM

Theoretically we demonstrated that reflection-based FTIR microspectroscopic data can be transformed into absorbance-like spectra through spectral extrapolation and a Kramers-Kronig transformation, where factors such as surface polishing, angle of incidence, and IR polarization should be considered. In addition, we validated reflection-based FTIRM empirically by comparing transmission-based FTIRM results from 4 μm thick bone sections with reflection-based FTIRM data from the matching polished bone blocks (Figure 5).

The light micrograph of an imaged area is shown in Figure 5B. The mineralization, collagen cross-linking, carbonate substitution and crystallinity profiles of a thin section and matching bone block are shown in Figures 5C-F. The peak frequencies and spectral integration parameters (Table 1) for the transmission and reflection data were compared using second derivative spectra. Absorption peak frequencies in the 1800 – 1300 cm^{-1} region were shifted by < 2 cm^{-1} for transmission- and reflection-based analysis so the integration ranges for these parameters were not adjusted (Figure 6A). However, due to a smaller amount of line broadening of the ν_3 PO_4^{3-} in the reflection spectra, the non-stoichiometric apatite peak at 1021 cm^{-1} and the stoichiometric apatite peak at 1032 cm^{-1} in the transmission spectra were shifted to 1025 and 1035 cm^{-1} in the reflection spectra, respectively (Figures 6B and 6C).

When comparing the percent difference between transmission and reflection FTIRM (Table 2), the mineralization, carbonate incorporation, and collagen cross-linking varied by 7 – 9%, while the difference in crystallinity was higher at 16%. Table 2 shows the coefficients of variation (CV) for each parameter, which represent a measure of specimen-to-specimen variation. For both transmission and reflection FTIRM, the collagen cross-linking, mineralization, and carbonate incorporation showed a 7 – 10% variation between different bone specimens. The crystallinity was much more consistent between specimens, with a CV value of only 2 – 3%.

DISCUSSION

Fractures of the skeleton are directly related to a deterioration of bone strength. However, it has become clear that fractures cannot be explained as a simple decrease in bone quantity (i.e. bone mineral density), but are also significantly dependent upon bone quality. While a formal definition of bone quality is somewhat elusive, mechanical tissue properties are a critical factor. As these mechanical properties will be greatly influenced by the chemical composition and ultrastructure of the tissue, methods that can readily correlate individual chemical, mechanical, and structural properties are necessary. To date, correlative studies such as these are typically performed across different specimens without performing the correlations on the same volume of tissue. While useful, this approach is limited by inter- and intra-specimen heterogeneity. In this study, we developed and demonstrated reflection-based FTIRM as an alternative approach to transmission-based FTIRM, enabling direct pixel-to-pixel correlations with other high resolution imaging modalities such as nanoindentation and qBSE on a single specimen, thereby providing accurate spatial associations between outcome measures.

We have shown theoretically that spectra produced by reflection-based FTIRM can be transformed into absorbance-like spectra using a Kramers-Kronig transform. These absorbance-like spectra can be analyzed with standard methods used for transmission-based FTIRM. Furthermore, no additional hardware is required for reflection FTIRM beyond what is already available for transmission FTIRM. The Kramers-Kronig transformation relies upon the measurement of the specular (non-diffuse) reflectance from the specimen surface. Specimen preparation consists of polishing the specimen and orienting its surface perpendicular to the normal of the incident IR beam to ensure that spectral data are collected

with high signal-to-noise. In order to ease handling and orient the bone properly for polishing, the specimen may be mounted and/or embedded.

We have shown empirically that reflection-based FTIRM can be used to determine the mineralization, crystallinity, carbonate substitution, and collagen cross-linking parameters that are equivalent to the transmission-based approach. Absorption peaks were shifted by < 2 cm^{-1} between the reflection and transmission datasets in the 1800 – 1300 cm^{-1} region. We observed 3 - 4 cm^{-1} shifts in absorbance maxima and a narrowing of the bandwidths for the non-stoichiometric and stoichiometric apatite peaks, suggesting that conventional Gaussian/ Lorentzian fits, which are presumed to be the best-fit distribution for standard transmission FTIRM, may not best describe spectral peaks obtained via reflection-based FTIRM. Rather, a more Gaussian-like band shape better describes the reflection data and may be attributed to a reduced natural and/or collision broadening in reflection-based FTIRM. [18]

One benefit of reflection-based FTIRM is that the technique does not require thin bone specimens, and thus sample embedding is not strictly required, although it may facilitate the handling of thick bone specimens and small bone blocks. While most human tissue specimens are already embedded for histology or histomorphometry, many specimens from pre-clinical studies are readily available and typically not embedded. For these specimens, a non-infiltrating embedding resin such as epoxy can be used to help orient and polish the sample. This process can be done overnight compared to several weeks for embedding in an infiltrating resin such as PMMA. The use of a non-infiltrating resin also avoids potential spectral overlap between the resin and bone and therefore removes the need for subtracting the resin spectrum at each pixel.

The use of thick bone specimens or small bone blocks also enables true pixel-to-pixel correlations with other imaging modalities such as nanoindentation, qBSE and/or a 2-D surface slice from a μCT reconstruction. It can also be correlated with Raman microscopy, which has been successfully been used to obtain chemical information on thick bone specimens and small bone blocks, but also on bulk bone and fresh, hydrated specimens. Raman microscopy can provide sub-micron spatial resolution, but data acquisition times are typically longer. [19]

Reflection-based FTIRM removes several possible sources of variability that can occur in transmission-based FTIRM, such as those introduced by specimen preparation and the cutting of thin sections. While reflection-based FTIRM provides an attractive alternative to the transmission-based approach, potential sources of error and factors that reduce signal-to-noise must be taken into careful consideration. First, in order to achieve the best signal-to-noise, the angle of incidence provided by the IR optics should be < 40°. If this angle is exceeded, or if the median angle approaches this value, the IR polarization should be predominantly *s*-polarized. Second, the specimen should be polished to a flat and specular reflecting surface. Third, spectral processing of reflection spectra into their equivalent absorption spectra is performed using algorithms in commercially available software, and requires that spectra be extended beyond the peaks of interest. In the case of bone, the $\nu_{1,}\nu_3$ PO_4^{3-} peak will not be properly resolved if this condition is not met.

One limitation of the empirical validation of this study arises from the fact that the regions probed for the transmission and reflection measurements were not identical. Since it was necessary to polish the bone block after cutting the thin sections, the sampled regions were offset by 54±12 μm in the mediolateral plane, a length scale at which chemical variations can exist. Small differences in the homogeneity of biochemical components will lead to small differences in the spectroscopic data. [19] However, the bones analyzed were from the cortical shell of the mid-diaphysis of mature mouse femurs, which are not undergoing

significant bone metabolism, limiting the spatial heterogeneity. Nonetheless, the magnitude of the variations between the sampled regions of the polished bone block and the thin sections was well within the range of inherent bone specimen heterogeneity, both spatially within one specimen and between specimens. Thus, the observed chemical differences between the transmission and reflection measurements were possibly due to the ~54 μm displacement between the sampled regions.

CONCLUSIONS

In summary, we anticipate that reflection-based FTIRM will more readily allow the pixel-to-pixel correlations within a single specimen between bone's material, mechanical, and morphological properties on the micron (and perhaps nano) scale by combining FTIRM with techniques such as nanoindentation, Raman microscopy, qBSE, and 2-D surface slices from μCT reconstructions. These investigations may elucidate how region-specific differences in bone chemistry – caused by metabolic, genetic, environmental, or structural influences – affect the microscopic material properties of bone tissue and alter the local mechanical behavior. As such, this spatially-resolved, correlative approach will significantly contribute to a better understanding of the contributors to bone quality and fracture risk.

Supplementary Material

Refer to Web version on PubMed Central for supplementary material.

Acknowledgments

This work was funded by the National Institutes of Health grant AR052778 and Brookhaven National Laboratory's Laboratory Directed Research and Development (LDRD) program (07-089). The National Synchrotron Light Source is supported by the U.S. Department of Energy under Contract No. DE-AC02-98CH10886. Matlab routine is available upon request.

REFERENCES

(1). Judex S, Boyd S, Qin YX, Miller L, Muller R, Rubin C. Curr Osteoporos Rep. 2003; 1:11–19. [PubMed: 16036060]

(2). Miller LM, Little W, Schirmer A, Sheik F, Busa B, Judex S. Journal of Bone and Mineral Research. 2007; 22:1037–1045. [PubMed: 17402847]

(3). Donnelly E, Chen DX, Boskey AL, Baker SP, van der Meulen MC. Calcif Tissue Int. 2010; 87:450–460. [PubMed: 20730582]

(4). Isaksson H, Malkiewicz M, Nowak R, Helminen HJ, Jurvelin JS. Bone. 2010; 47:1030–1038. [PubMed: 20813215]

(5). Burket J, Gourion-Arsiquaud S, Havill LM, Baker SP, Boskey AL, van der Meulen MC. J Biomech. 2011; 44:277–284. [PubMed: 21074774]

(6). Gourion-Arsiquaud S, Burket JC, Havill LM, DiCarlo E, Doty SB, Mendelsohn R, van der Meulen MC, Boskey AL. J Bone Miner Res. 2009; 24:1271–1281. [PubMed: 19210217]

(7). Bala Y, Farlay D, Delmas PD, Meunier PJ, Boivin G. Bone. 2010; 46:1204–1212. [PubMed: 19969115]

(8). Brennan O, Kennedy OD, Lee TC, Rackard SM, O'Brien FJ, McNamara LM. J Biomech. 2011; 44:386–390. [PubMed: 21093863]

(9). Gourion-Arsiquaud S, Faibish D, Myers E, Spevak L, Compston J, Hodsman A, Shane E, Recker RR, Boskey ER, Boskey AL. Journal of Bone and Mineral Research. 2009; 24:1565–1571. [PubMed: 19419303]

(10). Boskey A, Spevak L, Weinstein R. Osteoporosis International. 2009; 20:793–800. [PubMed: 18769963]

(11). Pleshko N, Boskey A, Mendelsohn R. Calcified Tissue International. 1992; 51:72–77. [PubMed: 1393781]

(12). Aparicio S, Doty SB, Camacho NP, Paschalis EP, Spevak L, Mendelsohn R, Boskey AL. Calcified Tissue International. 2002; 70:422–429. [PubMed: 12055658]

(13). Paschalis EP, DiCarlo E, Betts F, Sherman P, Mendelsohn R, Boskey AL. Calcif Tissue Int. 1996; 59:480–487. [PubMed: 8939775]

(14). Ou-Yang H, Paschalis EP, Mayo WE, Boskey AL, Mendelsohn R. Journal of Bone and Mineral Research. 2001; 16:893–900. [PubMed: 11341334]

(15). Paschalis EP, Betts F, DiCarlo E, Mendelsohn R, Boskey AL. Calcif Tissue Int. 1997; 61:480–486. [PubMed: 9383275]

(16). Paschalis EP, Verdelis K, Doty SB, Boskey AL, Mendelsohn R, Yamauchi M. J Bone Miner Res. 2001; 16:1821–1828. [PubMed: 11585346]

(17). Lucarini, V.; Saarinen, JJ.; Peiponen, K-E.; Vartiainen, EM. Kramers-Kronig Relations in Optical Materials Research. Springer; Berlin: 2005.

(18). Allara DL, Baca A, Pryde CA. Macromolecules. 1978; 11:1215–1220.

(19). Davis BJ, Carney PS, Bhargava R. Anal Chem. 2010; 82:3487–3499. [PubMed: 20392064]

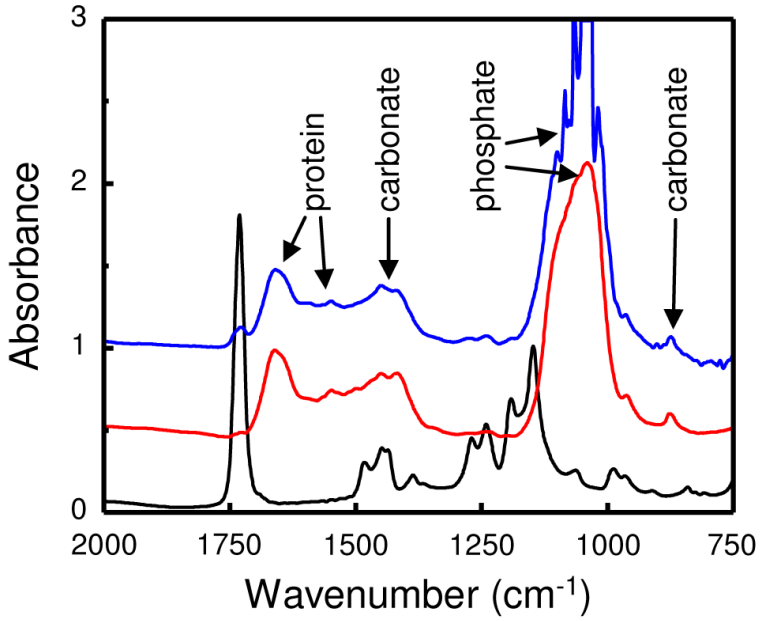

Figure 1.
(Red) A typical FTIRM spectrum of bone showing the characteristic protein and mineral components. (Blue) A FTIRM spectrum taken from a bone section that is too thick, illustrating detector saturation at the $\nu_1\nu_3$ phosphate peak. (Black) The FTIR spectrum of the embedding medium, PMMA, showing peaks that overlap with the bone spectrum. Spectra were offset by 0.5 absorbance units for clarity.

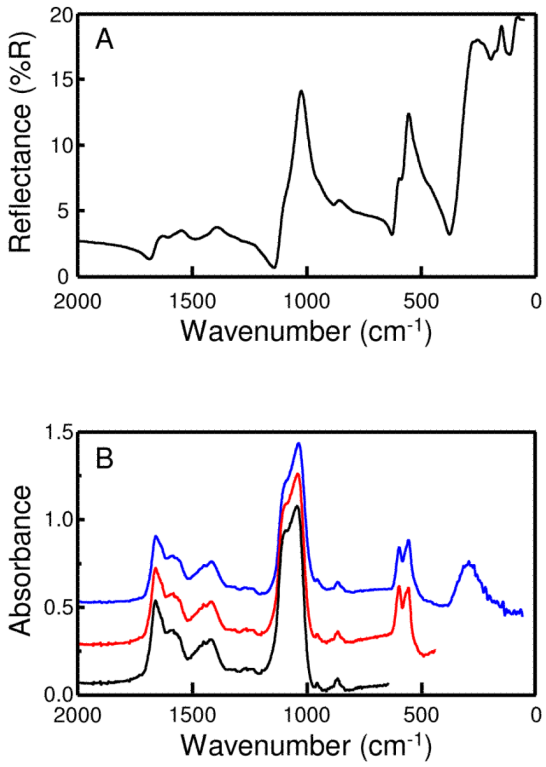

Figure 2.
(A) A FTIRM spectrum of a mineralized bone block collected in a reflection geometry. (B) FTIRM absorbance spectra calculated from the reflectance data in (A) with a low-frequency cutoff at 650 (black), 400 (red) and 70 cm^{-1} (blue). Spectra were offset by 0.25 absorbance units for clarity.

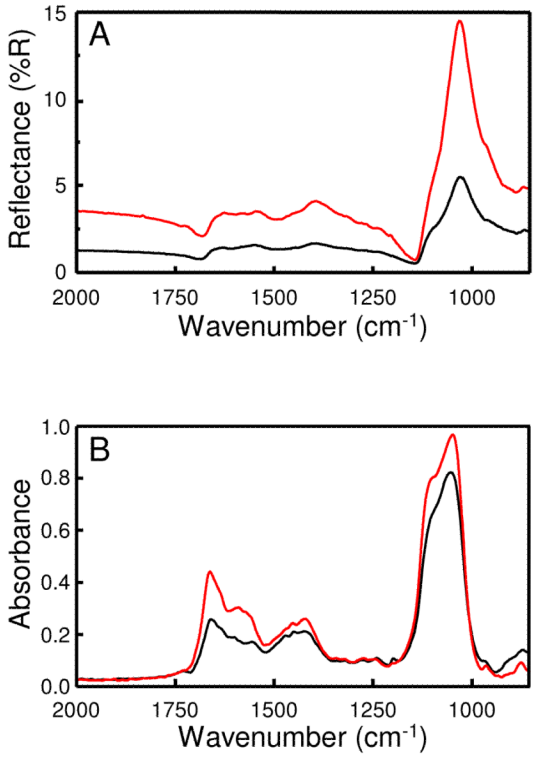

Figure 3.
(A) FTIRM reflectance spectra of a polished (red) and unpolished (black) bone block. The polished bone block has a net reflectance nearly double that of the unpolished block over the entire range of the spectrum. (B) FTIRM absorbance spectra calculated from the reflectance data in (A). The polished bone block (red) has a higher absorbance than the unpolished block (black), consistent with the increased reflectance as seen in (A). However, the relative peak intensities are not affected by the quality of polishing.

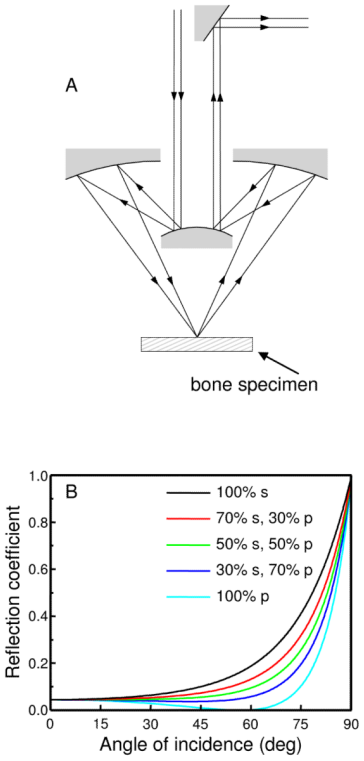

Figure 4.

(A) Schematic overview of the reflection geometry configuration using a Schwarzschild objective typically employed in IR microscopes. The central obscuration limits the half angle to a range between 15 - 40°. (B) Plot of the reflection coefficient versus angle of incidence as a function of polarization for hydroxyapatite (n=1.530). The reflection coefficient changes as a function of angle of incidence, but remains sufficiently constant out to 40° such that is does not measurably affect analysis.

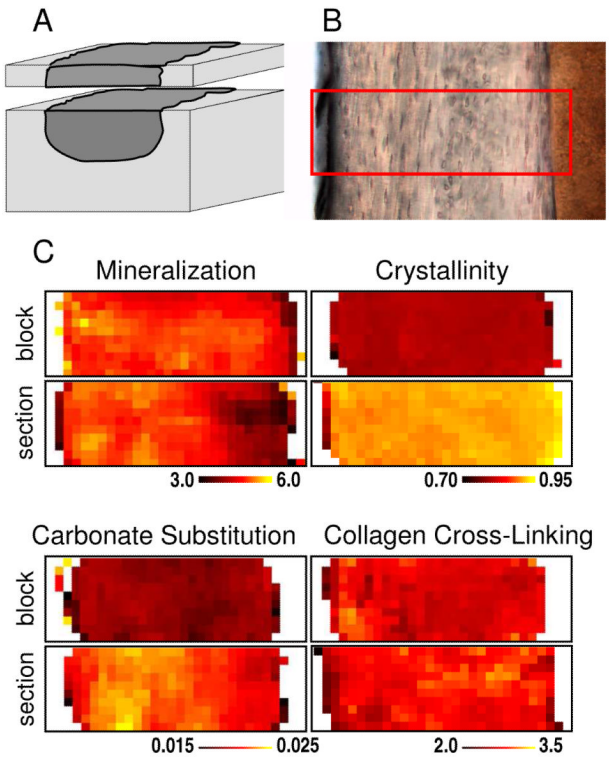

Figure 5.
(A) Schematic of specimen preparation. Thin sections were cut from the top surface of the bone block and imaged in a transmission geometry. The bone block was then imaged before and after polishing. (B) Light micrograph of an embedded and polished bone specimen with the highlighted area showing the region that was scanned using reflection FTIRM. (C) Integration maps showing the distribution of mineralization, crystallinity, carbonate substitution and collagen cross-linking for matching bone blocks and thin sections.

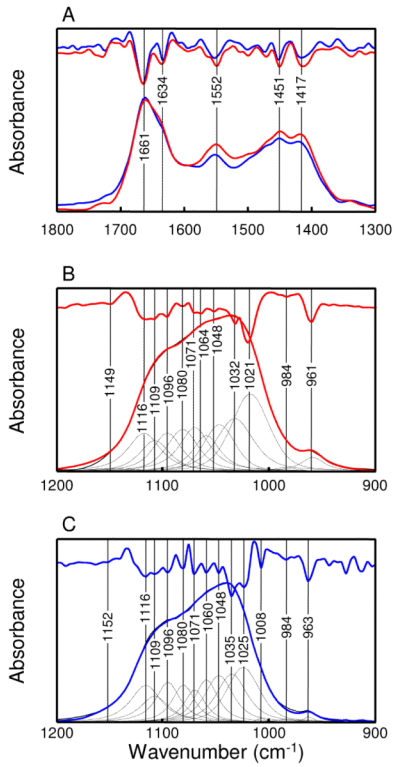

Figure 6.

(A) Transmission (red) and reflection-derived (blue) absorbance spectra and second-derivative spectra showing identical peak positions of the amide I, amide II, and CO^{2-}_3 bands. Curve-fitting of the ν_1,ν_3 PO_4^{3-} domain from (B) transmission and (C) reflection spectra based on peak positions from second-derivative spectra. Individual Gaussian/Lorentzian distributions and the resultant spectrum are also shown (black). The stoichiometric and non-stoichiometric apatite peaks are shifted from 1032 and 1021 cm^{-1} in the transmission spectrum to 1035 and 1025 cm^{-1} in the reflection-derived absorbance spectrum.

Table 1

Chemical parameters and associated spectral ranges used for integrating transmission and reflection derived absorbance spectra.

IR Parameter	Transmission mode integration range (cm^{-1})	Reflection mode integration range (cm^{-1})	Baseline (cm^{-1})
Collagen cross-linking[16]	(1661-1659) / (1691-1689)	(1661-1659) / (1691-1689)	1800 - 1300
Crystallinity[15]	(1034-1030) / (1023-1019)	(1037-1033) / (1027-1023)	1200 - 900
Protein	1700 - 1600	1700 – 1600	1800 - 1300
Phosphate	1200 - 900	1200 – 900	1200 - 900
Carbonate	1424 - 1414	1424 – 1414	1800 - 1300
Mineralization[13]	phosphate / protein	phosphate / protein	
Carbonate substitution[14]	carbonate / phosphate	carbonate / phosphate	

Table 2

Mean values ± standard deviations and CV for FTIRM spectral parameters from transmission FTIRM through a 4 μm bone thin section and reflection FTIRM from the matching bone block.

IR Parameter	Specimen #	Thin section		Polished block		% Difference
		Mean	CV	*Mean*	*CV*	
Collagen cross-linking	Specimen 1	2.285 ± 0.158	6.91%	2.671 ± 0.230	8.61%	+16%
	Specimen 2	2.287 ± 0.141	6.17%	2.439 ± 0.201	8.24%	+6%
	Specimen 3	2.438 ± 0.414	16.98%	2.545 ± 0.103	4.05%	+4%
	Average		**10.02%**		**6.97%**	**+9%**
Crystallinity	Specimen 1	1.111 ± 0.031	2.80%	1.214 ± 0.021	1.73%	+9%
	Specimen 2	1.090 ± 0.019	1.74%	1.351 ± 0.028	2.07%	+21%
	Specimen 3	1.072 ± 0.040	3.73%	1.271 ± 0.024	1.89%	+17%
	Average		**2.76%**		**1.90%**	**+16%**
Mineralization	Specimen 1	4.982 ± 0.247	4.96%	4.297 ± 0.231	5.38%	−15%
	Specimen 2	5.203 ± 0.449	8.63%	5.178 ± 0.363	7.01%	−0%
	Specimen 3	5.267 ± 0.474	9.00%	4.973 ± 0.264	5.31%	−6%
	Average		**7.53%**		**5.90%**	**−7%**
Carbonate Substitution	Specimen 1	0.020 ± 0.001	5.00%	0.021 ± 0.001	4.76%	+5%
	Specimen 2	0.022 ± 0.001	4.55%	0.020 ± 0.001	5.00%	−10%
	Specimen 3	0.024 ± 0.003	12.50%	0.019 ± 0.001	5.26%	−23%
	Average		**7.35%**		**5.01%**	−9%